IOPscience iopscience.iop.org

Home Search Collections Journals About Contact us My IOPscience

Fabrication and characteristics of a GaN-based microcavity laser with shallow etched mesa

This content has been downloaded from IOPscience. Please scroll down to see the full text.

2014 Appl. Phys. Express 7 062101

(http://iopscience.iop.org/1882-0786/7/6/062101)

View the table of contents for this issue, or go to the journal homepage for more

Download details:

IP Address: 140.113.38.11
This content was downloaded on 25/12/2014 at 02:57

Please note that terms and conditions apply.

Applied Physics Express 7, 062101 (2014)
http://dx.doi.org/10.7567/APEX.7.062101

Fabrication and characteristics of a GaN-based microcavity laser with shallow etched mesa

Ying-Yu Lai, Yu-Hsun Chou, Yu-Sheng Wu, Yu-Pin Lan, Tien-Chang Lu*, and Shing-Chung Wang

Department of Photonics, National Chiao Tung University, Hsinchu 300, Taiwan
E-mail: timtclu@mail.nctu.edu.tw

Received April 15, 2014; accepted April 21, 2014; published online May 14, 2014

In this work, we have developed a simple GaN-based microcavity (MC) with an intracavity shallow etched mesa. The textured GaN-based MC incorporated two high-reflectivity dielectric Bragg mirrors and an InGaN/GaN multiple quantum well with a shallow etched mesa as an optical confined structure. Lasing and transverse optical confinement characteristics have been verified by measuring devices with different mesa diameters. A quality factor (Q) of 2600 and a threshold energy of 30 nJ have been observed in a 10-μm-diameter device. Such a cavity structure could be implanted into electrically pumped GaN vertical-cavity surface-emitting lasers for supporting efficient transverse confinement.
© 2014 The Japan Society of Applied Physics

Planar microcavities (MCs) embedded with a semiconductor active layer have been utilized in various optoelectronic applications, especially laser devices. A typical example is the vertical-cavity surface-emitting lasers (VCSELs), which are driven by photonic stimulated emission.[1] As the active layer exhibits a strong excitonic feature, the MC could enter into the strong coupled polaritonic regime through strong exciton–photon coupling and achieve an ultralow-threshold polariton laser through the polaritonic stimulated scattering.[2] Among so many semiconductor materials, GaN and its ternary and quaternary alloys are regarded as the most popular material systems for novel MC polaritonic emitters and vertical-cavity laser devices owing to their large exciton binding energy (~26 meV) and wide spectral tuning range in the ultraviolet–visible region.[3,4] Generally, the GaN-based MCs could be divided into three major types from their distributed Bragg reflector (DBR) compositions: all-epitaxial, epitaxial-dielectric hybrid, and all-dielectric.[5–11] So far, the optically pumped polariton lasers, electrically pumped VCSELs, and polariton LEDs have been demonstrated using planar GaN-based hybrid MCs.[12–14] However, the efficient lateral optical confinement among these devices is still lacking and limiting their performance. In 2011, Cheng et al. successfully achieved a high-quality-factor (Q) MC light emitter with sufficient lateral optical/electrical confinement using an intracavity AlN aperture.[15] Unfortunately, the insertion of AlN apertures may cause additional unexpected damage to the multiple quantum well (MQW) owing to their higher regrowth temperature. In the GaAs system, the lateral optical confinement could be easily achieved using an etched micropillar or a micropillar embedded into BCB.[16,17] However, it is hard to etch down a whole GaN micropillar cavity owing to the difficult etching process of the III–nitride system. In view of this, the surface-textured structure would be a better way to introduce a sufficiently large index contrast for lateral optical confinement without causing damage to the gain medium in the VCSELs or MC devices. Such a technique has recently been demonstrated in an electrically pumped GaAs MC emitter for tailoring the three-dimensional photonic confinement, but has not yet been reported in the GaN-based MC system.[18]

In this letter, we demonstrate a GaN-based all-dielectric MC with in-plane optical confinement using a shallow etched mesa structure. The all-dielectric MC provides a wide range of high-reflectivity stopbands for flexibility in the fabrication process. The shallow etched mesa structure presents a sufficient lateral optical confinement owing to its higher effective refractive index. The multi-transverse mode spectra show the lateral confinement of the proposed shallow etched mesa structure. In addition, the device with a larger mesa diameter has a higher Q value and a lower threshold density owing to its smaller diffraction loss and scattering loss.

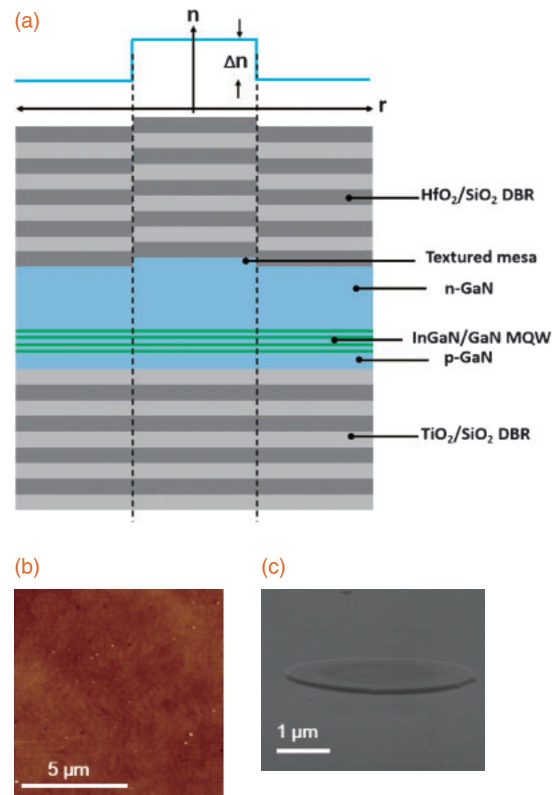

Fig. 1. (a) Schematic diagram of textured GaN-based MC structure and corresponding effective refractive index distribution. (b) A $10 \times 10\,\mu m^2$ AFM scan of an n-GaN surface after polishing. (c) Scanning electron microscopy (SEM) image of textured mesa on n-GaN surface.

Figure 1(a) shows the schematic diagram of the proposed textured GaN-based MC. The original cavity layers were grown by metal organic chemical vapor deposition (MOCVD) on a (0001) c-plane sapphire substrate, followed by a 30 nm GaN nucleation layer at 500 °C, a 2 μm undoped GaN (u-GaN) spacer at 1100 °C, a 2 μm n-GaN layer, 10 pairs of $In_{0.1}Ga_{0.9}N$ (2 nm)/GaN (10 nm) MQWs, and a 150 nm p-GaN spacer. An 11.5-pair TiO_2/SiO_2 DBR was deposited on top of the p-GaN spacer using an E-gun deposition

 © 2014 The Japan Society of Applied Physics

system and was adhered onto a silica substrate. Then, the sample was removed from the sapphire substrate using the laser lift-off (LLO) technique.[19] The corresponding root-mean-square (rms) roughness of the lifted-off u-GaN surface was about 10 nm. Then, the thickness of the u-GaN and n-GaN layers was reduced to about 2 μm by inductively coupled plasma reactive ion etching (ICP-RIE) and polishing. The thickness of the cavity layer was mainly controlled by ICP-RIE since the polishing slurry diameter employed was small and sufficient for planarization. The surface roughness of the exposed n-GaN layer was measured to be 1 nm from the $10 \times 10\,\mu m^2$ atomic force microscopy (AFM) scan after polishing, as shown in Fig. 1(b). Before depositing the n-side DBR, a series of circular mesas of 60 nm height and varying diameters had been patterned and etched on the polished n-GaN by photolithography and ICP-RIE dry etching, respectively, as shown in Fig. 1(c). These textured mesas provide a step index contrast (Δn) for the transverse mode guiding, as shown on the top side of Fig. 1(a). Finally, the n-side DBR consisting of 11.5 pairs of SiO_2 and HfO_2 quarter-wavelength stacks was deposited on the n-GaN surface. HfO_2 was used owing to its low absorption in the UV region, which helps to increase the pumping efficiency for the following measurements. Both the TiO_2/SiO_2 and HfO_2/SiO_2 DBRs show high reflectivities (>99.5%) at the MQW emission wavelength (430 nm), which assure a high-finesse optical MC structure. The optical measurements of all-dielectric GaN-based textured MCs were performed at room temperature (RT) using a third-harmonic generation (THG) of a Nd:YVO_4 laser with a 355 nm emission wavelength (outside the stopband of the top HfO_2/SiO_2 DBR) and a 1 kHz repetition rate. The pumping beam and cavity emission were focused to about 10 μm and collected via a 40× objective lens with a numerical aperture of 0.5, respectively.

Figure 2(a) shows the cavity emission from a textured device of 8 μm diameter under various pumping conditions. Below the threshold energy (E_{th}), the spectrum exhibits a multi-longitudinal-mode characteristic owing to the relatively large cavity length. The measured mode spacing between the longitudinal modes is about 16 nm, which reflects a 2 μm cavity length. A magnified spectrum measured under $0.9E_{th}$ pumping condition is shown in the inset of Fig. 2(a) for a clearer specification. The magnified spectrum comprises several peaks that come from the transverse confinement of a circular shallow etched mesa. Δn of about 0.068 between the circular shallow etched mesa and the peripheral area could be easily calculated from the effective index model (EIM).[20] From the calculation, Δn could range from 0.011 to 0.1151 as the mesa height increases from 10 to 100 nm. Such a wide tuning range of index contrast promises a powerful technique for manipulating the transverse optical confinement in GaN-based MCs. In addition, the shallow etched mesa height is feasible to process at p-GaN of an electrically pumped GaN-based VCSEL to act as the current confinement aperture.[21] Figure 2(b) shows a clear evolution of the output intensity and mode linewidth versus the pumping energy. The output laser intensity from the sample shows a nonlinear increase, and the linewidth presents a sharp narrowing as the pumping energy across the threshold ($E_{th} = 130$ nJ). The Q value estimated below the threshold is about 1300.

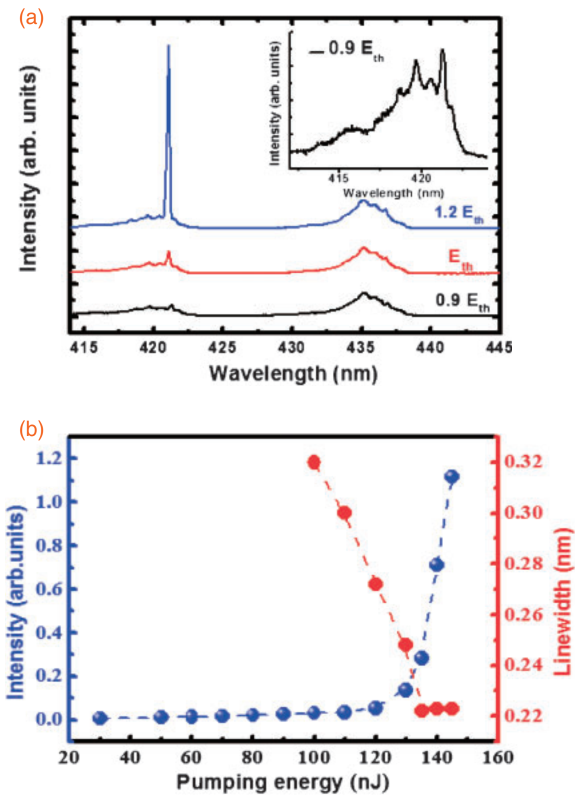

Fig. 2. (a) Measured spectra of textured GaN VCSEL of 8 μm diameter under various pumping energies. (b) Output intensity and peak linewidth as functions of pumping energy. The inset in (a) shows a magnified spectrum under $0.9E_{th}$ pumping condition.

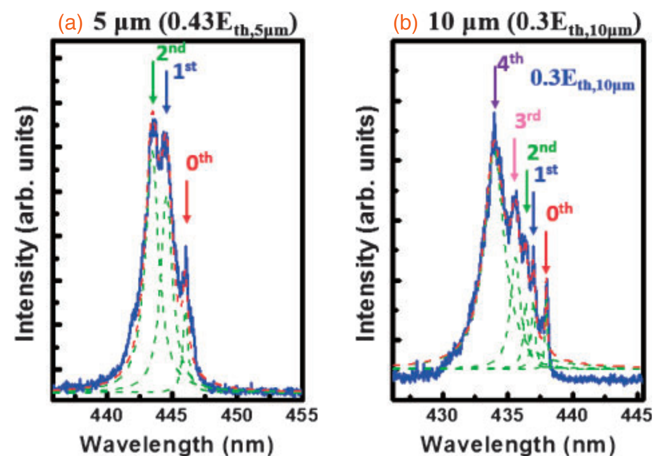

Fig. 3. Spectra of (a) 5 and (b) 10 μm textured-mesa devices (blue curve) below the threshold condition. Green dashed lines represent the fitting curves of each transverse optical mode, and red dashed lines depict the summarized fitting curves.

Figures 3(a) and 3(b) show the measured cavity emission spectra of 5 and 10 μm textured apertures (blue curve) far below the threshold for avoiding the linewidth to be affected by the stimulated emission. The spectrum of the 8 μm case is shown in the inset of Fig. 2(a). The finite central wavelength offset among devices with different mesa diameters is mainly attributed to an unavoidable thickness gradient during the epitaxial growth and lapping process. It is interesting to see that lower order modes show a narrower linewidth and

© 2014 The Japan Society of Applied Physics

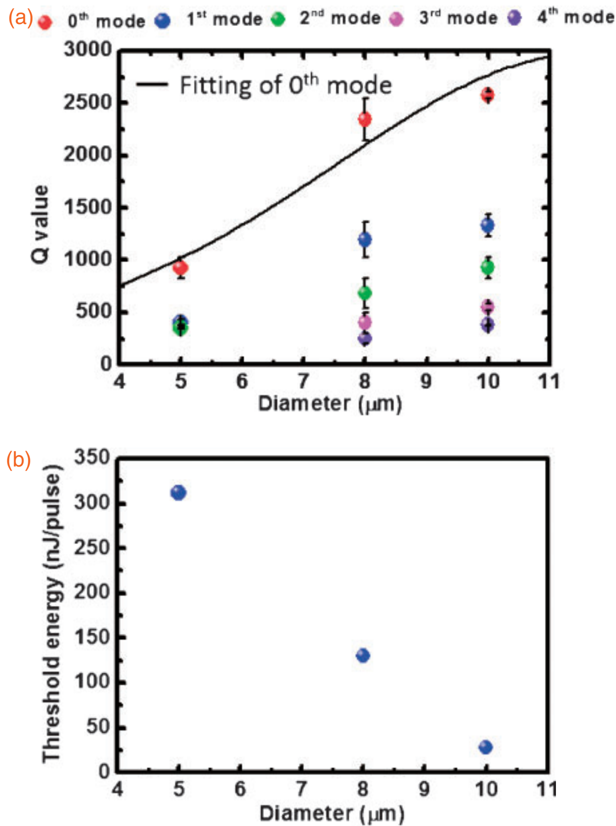

Fig. 4. (a) Estimated Q values with mode order of 5, 8, and 10 μm textured-mesa devices. (The black line represents the Q value fitting curve of the 0th mode.) (b) Threshold energy as a function of textured mesa diameter.

a higher Q value. This could be attributed to the sidewall roughness of the shallow etched mesa, which would introduce additional scattering loss to high-order transverse modes whose profiles are expanding to the edge of the aperture.

The estimated Q values of each transverse confined optical mode are shown in Fig. 4(a). The fundamental modes (0th) with different aperture sizes have the highest Q value owing to a weaker scattering loss impact. The mode distribution of higher order modes becomes more disperse and closer to the mesa edge, and would result in a larger scattering loss and a lower Q value, as shown in Fig. 4(a). The Q value of the 10-μm-diameter device can reach as high as 2600, which is twice larger than that in the 5 μm case. The reduction in Q value among smaller aperture sizes is attributed to its edge scattering loss and higher diffraction loss. The Q value of the device with radius a is modulated owing to additional scattering loss at the shallow mesa edge and could be easily simulated using a simple model $1/Q(a) = 1/Q_0 + 1/Q_{\text{scattering}}$, where Q_0 is the planar MC quality factor and $Q_{\text{scattering}}$ is the scattering term.[22] Taking the fundamental transverse mode distribution that follows the first Bessel function $J_0(k_t a)$, for example, where $k_t^2 = k_0^2 n_{\text{eff}}^2 - \beta^2$, n_{eff} being the effective core index calculated from the EIM model and β the propagation constant, the aforementioned model could be expressed as $1/Q(a) = 1/Q_0 + \varepsilon(J_0^2(k_t a))/a$, where ε is a phenomenological proportionality constant. The experimental data are fitted with this model [black curves in Fig. 4(a)], giving a planar Q value of 3000 and a ε of $5.5 \times 10^{-8}\,\mu\text{m}^{-1}$. Furthermore, the high Q value of larger devices also shows a significant impact on reducing the threshold energy. The threshold density can be reduced tenfold if the mesa diameter increases from 5 to 10 μm. To specify the impact of mesa diameter on the MC device performance, the threshold energies are plotted as a function of aperture diameter, as shown in Fig. 4(b).

In conclusion, we have demonstrated all-dielectric GaN-based MCs with efficient lateral optical confinement using shallow etched circular mesas. The optical confinement can be achieved using the index contrast induced by the textured mesa. For comparison, a device with a larger mesa diameter has a smaller mode spacing, a larger Q value, and a lower threshold density. A high Q value of 2600 and a low threshold energy of 30 nJ could be achieved in the device with a 10 μm mesa diameter. Such a high-Q GaN-based MC structure is very promising for tailoring the strong light-matter interaction and fundamental research, such as polaritonic physics.[14] For a more practical application, our proposed GaN-based MC with shallow etched mesa structures can also be utilized nowadays in electrically pumped GaN-based VCSELs serving as a current confinement aperture for realizing a more efficient operation. To further enhance the device performance, the innate scattering loss induced by the sidewall roughness could be minimized by properly adjusting the photoresist profile and dry etching condition or using wet etching in the future.[23] Other practical functions, such as polarization control, can be achieved by changing the circular mesa into a grating structure. Our demonstration provides a powerful solution for manipulating the optical modes and could be applied to future GaN-based MC devices such as polaritonic emitters and VCSELs.

Acknowledgments The authors would like to gratefully acknowledge Professor H. C. Kuo at National Chiao Tung University for technical support and would like to acknowledge DISCO Corporation in Tokyo for the high-quality LLO process. This work has been supported in part by the MOE ATU program and in part by the National Science Council of the Republic of China in Taiwan under Contract Nos. NSC 100-2628-E-009-013-MY3 and NSC 102-2221-E-009-156-MY3.

1) K. Iga, IEEE J. Sel. Top. Quantum Electron. **6**, 1201 (2000).
2) H. Deng, G. Weihs, D. Snoke, J. Bloch, and Y. Yamamoto, Proc. Natl. Acad. Sci. U.S.A. **100**, 15318 (2003).
3) F. A. Ponce and D. P. Bour, Nature **386**, 351 (1997).
4) G. Malpuech, A. D. Carlo, A. Kavokin, J. J. Baumberg, M. Zamfirescu, and P. Lugli, Appl. Phys. Lett. **81**, 412 (2002).
5) J. M. Redwing, D. A. S. Loeber, N. G. Anderson, M. A. Tischler, and J. S. Flynn, Appl. Phys. Lett. **69**, 1 (1996).
6) T. C. Lu, C. C. Kao, H. C. Kuo, G. S. Huang, and S. C. Wang, Appl. Phys. Lett. **92**, 141102 (2008).
7) T. C. Lu, S. W. Chen, T. T. Wu, P. M. Tu, C. K. Chen, C. H. Chen, Z. Y. Li, H. C. Kuo, and S. C. Wang, Appl. Phys. Lett. **97**, 071114 (2010).
8) Y. Higuchi, K. Omae, H. Matsumura, and T. Mukai, Appl. Phys. Express **1**, 121102 (2008).
9) K. Omae, Y. Higuchi, K. Nakagawa, H. Matsumura, and T. Mukai, Appl. Phys. Express **2**, 052101 (2009).
10) T. Onishi, O. Imafuji, K. Nagamatsu, M. Kawaguchi, K. Yamanaka, and S. Takigawa, IEEE J. Quantum Electron. **48**, 1107 (2012).
11) K. S. Daskalakis, P. S. Eldridge, G. Christmann, E. Trichas, R. Murray, E. Iliopoulos, E. Monroy, N. T. Pelekanos, J. J. Baumberg, and P. G. Savvidis, Appl. Phys. Lett. **102**, 101113 (2013).
12) S. Christopoulos, G. Baldassarri Höger von Högersthal, A. J. D. Grundy, P. G. Lagoudakis, A. V. Kavokin, J. J. Baumberg, G. Christmann, R. Butté, E. Feltin, J.-F. Carlin, and N. Grandjean, Phys. Rev. Lett. **98**, 126405 (2007).

© 2014 The Japan Society of Applied Physics

13) G. Christmann, R. Butté, E. Feltin, J.-F. Carlin, and N. Grandjean, Appl. Phys. Lett. **93**, 051102 (2008).
14) T. C. Lu, J. R. Chen, S. C. Lin, S. W. Huang, S. C. Wang, and Y. Yamamoto, Nano Lett. **11**, 2791 (2011).
15) B. S. Cheng, Y. L. Wu, T. C. Lu, C. H. Chiu, C. H. Chen, P. M. Tu, H. C. Kuo, S. C. Wang, and C. Y. Chang, Appl. Phys. Lett. **99**, 041101 (2011).
16) S. Reitzenstein, C. Hofmann, A. Gorbunov, M. Strauß, S. H. Kwon, C. Schneider, A. Löffler, S. Höfling, M. Kamp, and A. Forchel, Appl. Phys. Lett. **90**, 251109 (2007).
17) C. Böckler, S. Reitzenstein, C. Kistner, R. Debusmann, A. Löffler, T. Kida, S. Höfling, A. Forchel, L. Grenouillet, J. Claudon, and J. M. Gérard, Appl. Phys. Lett. **92**, 091107 (2008).
18) K. Winkler, C. Schneider, J. Fischer, A. Rahimi-Iman, M. Amthor, A. Forchel, S. Reitzenstein, S. Höfling, and M. Kamp, Appl. Phys. Lett. **102**, 041101 (2013).
19) W. S. Wong, T. Sands, N. W. Cheung, M. Knesissl, D. P. Bour, P. Mei, L. T. Romano, and N. M. Johnson, Appl. Phys. Lett. **75**, 1360 (1999).
20) G. Ronald Hadley, Opt. Lett. **20**, 1483 (1995).
21) E. Hashemi, J. Gustavsson, J. Bengtsson, M. Stattin, G. Cosendey, N. Grandjean, and A. Haglund, Jpn. J. Appl. Phys. **52**, 08JG04 (2013).
22) T. Rivera, J.-P. Debray, J. M. Gérard, B. Legrand, L. Manin-Ferlazzo, and J. L. Oudar, Appl. Phys. Lett. **74**, 911 (1999).
23) S. Y. Bae, D. J. Kong, J. Y. Lee, D. J. Seo, and D. S. Lee, Opt. Express **21**, 16854 (2013).

© 2014 The Japan Society of Applied Physics